Journal of
Synchrotron Radiation

ISSN 0909-0495

Received 19 February 2013
Accepted 6 May 2013

X-ray absorption study of the local structure at the NiO/oxide interfaces

Iulian Preda,[a] Leonardo Soriano,[a]* Daniel Díaz-Fernández,[a] Guillermo Domínguez-Cañizares,[a] Alejandro Gutiérrez,[a] Germán R. Castro[b,c] and Jesús Chaboy[d,e]

[a]Departamento de Física Aplicada and Instituto de Ciencia de Materiales Nicolás Cabrera, Universidad Autónoma de Madrid, Cantoblanco, 28049 Madrid, Spain, [b]SpLine CRG BM25 Beamline, European Synchrotron Radiation Facility, 6 rue Jules Horowitz, BP 220, Grenoble 38043, France, [c]Instituto de Ciencia de Materiales de Madrid, Sor Juana Inés de la Cruz 3, Madrid 28049, Spain, [d]Instituto de Ciencia de Materiales de Aragón, Consejo Superior de Investigaciones Científicas, Universidad de Zaragoza, 50009 Zaragoza, Spain, and [e]Departamento de Física de la Materia Condensada, Universidad de Zaragoza, E-50009 Zaragoza, Spain.
E-mail: l.soriano@uam.es

This work reports an X-ray absorption near-edge structure (XANES) spectroscopy study at the Ni *K*-edge in the early stages of growth of NiO on non-ordered SiO_2, Al_2O_3 and MgO thin films substrates. Two different coverages of NiO on the substrates have been studied. The analysis of the XANES region shows that for high coverages (80 Eq-ML) the spectra are similar to that of bulk NiO, being identical for all substrates. In contrast, for low coverages (1 Eq-ML) the spectra differ from that of large coverages indicating that the local order around Ni is limited to the first two coordination shells. In addition, the results also suggest the formation of cross-linking bonds Ni—O—*M* (*M* = Si, Al, Mg) at the interface.

Keywords: XANES; oxide/oxide interfaces; NiO.

1. Introduction

The main aim of this work is to study the local symmetry of the Ni atoms located at the interfaces formed by the deposition of NiO thin films on selected oxides. Previous results on NiO/oxide interfaces studied by means of X-ray photoemission spectroscopy (XPS) have shown a strong interaction of the NiO layers with the most covalent substrates whereas this interaction is lower for ionic oxide substrates (Preda *et al.*, 2008). In general, these results suggest the formation of cross-linking bonds Ni—O—*M*, where *M* stands for the cation of the oxide substrate. However, to corroborate this conclusion, a more specific study of the geometrical symmetry of the Ni atoms at the interface has to be performed.

In this work we have studied the interface effects in the early stages of growth of NiO on three selected oxides, namely SiO_2, Al_2O_3 and MgO. The oxide substrates have been chosen according to the nature of their chemical bonding (from a more covalent to a more ionic character). Interesting trends in terms of covalency–ionicity of the substrates have already been observed in the study of the electronic structure of TiO_2/oxide interfaces with synchrotron radiation spectroscopies (Soriano *et al.*, 2000, 2011; Sánchez-Agudo *et al.*, 2001). We have also observed similar trends in NiO/oxide interfaces throughout the interpretation of the Ni 2*p* XPS spectra (Preda *et al.*, 2008).

The oxide substrates have been prepared as thin films following different conventional methods on conductive supports (see below). The MgO substrates were polycrystalline whereas those of SiO_2 and Al_2O_3 did not present a long-range order, being amorphous. Therefore, the use of a local structural probe such as X-ray absorption spectroscopy (XAS) renders very promising in the analysis of the NiO/oxide interface. Indeed, this scheme has been previously applied in the case of $Ni_xMg_{1-x}O$ solid solutions (Kuzmin *et al.*, 1995), magnetron-sputtered nickel oxide thin films (Kuzmin *et al.*, 1997; Anspoks & Kuzmin, 2011) and in crystallization studies of NiO nanoparticles (Meneses *et al.*, 2007). XAS has proven to be an outstanding structural tool by allowing the determination of the local environment around a selected atomic species in a great variety of systems (Sayers & Bunker, 1988). At present, reliable structural parameters are commonly derived from the analysis of the extended X-ray absorption fine-structure (EXAFS) region of the spectrum. Therefore we have recorded the Ni *K*-edge EXAFS signals of these samples for different stages of growth. However, the EXAFS-obtained spectra did not have sufficient quality for EXAFS analysis since the signal-to-noise ratio was low owing to the very small

amount of deposited material needed for the early stages study. The same applies to the occurrence of pre-edge structures, commonly addressed to off-site transitions, whose origin is presently under debate (Kuzmin *et al.*, 1995; Vedrinskii *et al.*, 2001; Gougoussis *et al.*, 2009). These drawbacks were overcome by studying the X-ray absorption near-edge structure (XANES) region of the spectra which exhibits, in all cases, sufficient quality to perform the aforementioned structural characterization of the NiO/oxide systems. Despite the fact that several studies have demonstrated that XANES is extremely sensitive to the stereochemical details of the absorbing site, *i.e.* overall symmetry, interatomic distances and bond angles (Díaz-Moreno *et al.*, 2000; Chaboy & Díaz-Moreno, 2011), offering even better capabilities than a direct EXAFS analysis for the determination of the coordination polyhedron around the absorbing atom (Chaboy & Díaz-Moreno, 2011; Díaz-Moreno & Chaboy, 2009), few structural determinations from XANES have been reported to date; the main reason being that the *ab initio* computation of XANES spectra is not so straightforward as for EXAFS, since XANES computation requires sophisticated simulation tools (Natoli & Benfatto, 1986; Ankudinov *et al.*, 1998; Joly, 2001).

Here we present a detailed study of the Ni *K*-edge XANES spectra in the case of NiO grown on SiO_2, Al_2O_3 and MgO. Comparison of the experimental spectra and *ab initio* computations has allowed us to determine the modification of the local structure of Ni in the early stages of growth of NiO on these oxides. Our results point out that for low coverages the local order around Ni extends only to the first two coordination shells. In addition, these results also suggest the presence of the substrate atoms at the interface, being consistent with the formation of Ni—O—*M* (*M* = Si, Al, Mg) cross-linking bonds at the NiO/oxide interface proposed from XPS experiments on the same systems (Preda *et al.*, 2008).

2. Experimental and computational methods

NiO was grown on the oxide substrates by reactive thermal evaporation of metallic Ni at room temperature in an oxygen atmosphere of 1×10^{-5} mbar. As mentioned above, we have used thin films of the oxides grown on conductive materials to avoid charging effects during measurements with synchrotron radiation. The silica substrate consisted of a 200 Å thin film of amorphous SiO_2 grown by dry oxidation of a p-doped Si (111) wafer. The Al_2O_3 substrate was an ultrathin film of thickness about 25 Å, grown by thermal oxidation of a pure polycrystalline Al foil at 623 K for 30 min. MgO was deposited *in situ* on a p-doped Si (111) wafer by reactive evaporation of Mg at room temperature in an oxygen atmosphere (1×10^{-5} mbar). It was not possible to deduce the thickness of the MgO thin film from the XPS intensities since it was much larger than the inelastic mean free path of the photoelectrons; however, it has been estimated as several micrometres from the atomic force microscopy (AFM) images (Preda *et al.*, 2008). Al_2O_3 and MgO substrates were prepared *in situ* previously to NiO deposition; thus they could be checked by XPS to detect for possible contamination. The SiO_2 substrate was prepared *ex situ*, being checked for contamination before the NiO growth process. All substrates were characterized by AFM measured in dynamic mode (tapping) using Nanotec's microscope and software (Horcas *et al.*, 2007). The RMS roughness was found to be very different for each substrate, ranging from 0.35 nm for the SiO_2 substrate to about 150 nm for the polycrystalline MgO substrate. In this case the relatively large roughness for the MgO substrate is produced by the formation of faceted crystallites of about 1 µm in size (Preda *et al.*, 2008). In spite of the substrates having a very different morphology, the extreme sensitivity of XANES to the local symmetry, rather than to long-range order, makes this technique very useful in the analysis of such systems.

The coverage and thickness of the NiO deposits were determined by quantitative analysis of the XPS inelastic peak shape following the technique described by Tougaard (1994) by means of the *QUASES* software. This technique is able to show the method of growth of a material on the support. According to this analysis, NiO showed the same method of growth on all substrates studied here through the Stransky–Krastanov-like mode, *i.e.* the growth of small islands of a determined height at the early stages of growth. Further details on the method of growth of NiO on these oxides can be found elsewhere (Preda *et al.*, 2008. Thus, the samples corresponding to one equivalent monolayer (1 Eq-ML) deposited on all oxide substrates consists of nanometric NiO islands of about 2 nm in height covering around 15% of the substrate surface whereas the 80 Eq-ML sample consisted of a NiO thin film of about 200 Å in thickness.

The XAS experiments were measured *ex situ* at the Ni *K*-edge ($E \simeq 8.3$ keV) at the SpLine BM25 experimental station of the European Synchrotron Radiation Facility (ESRF) in Grenoble, France. Measurements were carried out at room temperature in fluorescence mode, using a multi-element solid-state multichannel detector. The measurements were repeated at the KMC2 beamline of the synchrotron BESSY II, Berlin, Germany, in fluorescence mode. The spectra were similar to those obtained before, finding only differences in the signal-to-noise ratio. The XAS spectra were analyzed according to standard procedures (Sayers & Bunker, 1988) using the *ATHENA* program pack (Ravel & Newville, 2005).

The computation of the Ni *K*-edge XANES spectra was carried out by using the multiple-scattering code *CONTINUUM*, included in the *MXAN* program package (Benfatto & Longa, 2001), based on the one-electron full-multiple-scattering theory (Natoli & Benfatto, 1986). A complete discussion of the procedure can be found elsewhere (Chaboy & Quartieri, 1995; Chaboy, 2009; Chaboy *et al.*, 2005). The potential for the different atomic clusters was approximated by a set of spherically averaged muffin-tin potentials built by following the standard Mattheis' prescription. The muffin-tin radii were determined following Norman's criterion. During the computations, special attention was paid to determine the best choice for the overlapping factor between the muffin-tin spheres and for the exchange and correlation part of the final state potential (Chaboy *et al.*, 2007*a*,*b*; Hatada & Chaboy, 2007). The theoretically calculated spectra have been directly

compared with the experimental XANES spectrum, *i.e.* no fitting procedure has been used. Besides, no free parameters have been employed in the calculations, so the quality of the theoretical computations is based on the correct reproduction of the shape and energy position of the different spectral features and of their relative energy separation and the intensity ratio. In all of the cases the theoretical spectra have been convoluted with a Lorentzian shape function to account for the core-hole lifetime ($\Gamma = 1.5$ eV) (Krause & Oliver, 1979) and the experimental resolution.

3. Results and discussion

A comparison of the Ni *K*-edge absorption spectra for 80 Eq-ML is reported in Fig. 1. As expected, the absorption spectra of the 80 Eq-ML NiO samples are similar to that of bulk NiO (Anspoks & Kuzmin, 2011) and no dependence on the oxide substrate (SiO_2, Al_2O_3 and MgO) is observed. We have included in this figure the result of the *ab initio* XANES calculation for reference bulk NiO. By using this reference we have fixed the main ingredients of the computations that should be later applied to the case of the 1 Eq-ML samples. In this case we have performed the computation of the Ni *K*-edge XANES of NiO by using a cluster of 93 atoms, *i.e.* including the scattering contributions from neighbouring atoms located within the first 6 Å around the photoabsorbing Ni. During these calculations we have tested the performance of different exchange and correlation potentials (ECP) to account for the experimental spectrum. We have found that the best agreement between the computations and the experimental spectrum is obtained by using an overlapping factor of 1% and the Dirac–Hara ECP potential, in agreement with previous works for transition metal oxides (Guglieri & Chaboy, 2010; Guglieri *et al.*, 2011).

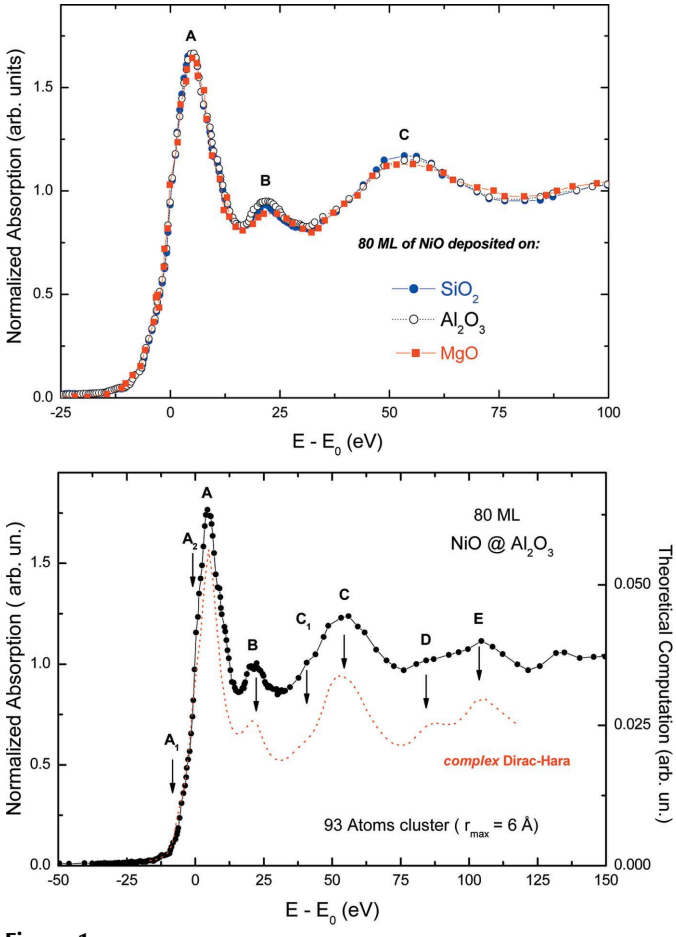

Figure 1
Top: experimental Ni *K*-edge XANES spectra for 80 Eq-ML of NiO deposited on SiO_2, Al_2O_3 and MgO. Bottom: comparison of the experimental spectrum of 80 Eq-ML of NiO on Al_2O_3 with the theoretical spectra calculated for bulk NiO (see text for details).

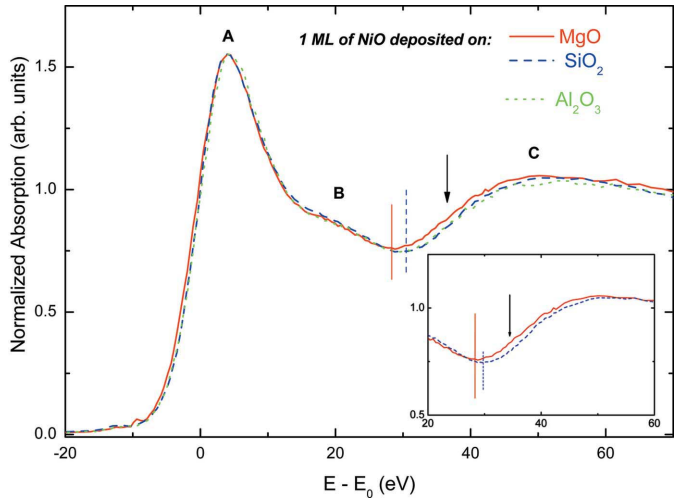

Figure 2
Comparison of the experimental Ni *K*-edge XANES spectra for 1 Eq-ML of NiO deposited on SiO_2, Al_2O_3 and MgO.

A comparison of the experimental Ni *K*-edge absorption spectra for the 1 Eq-ML samples is reported in Fig. 2. In this case the XANES spectra do not resemble that of bulk NiO but the absorption profile shows a strong smearing out of the main spectral features characteristic of a loss of local coordination around Ni. Indeed, the XANES spectra are quite similar to those of Ni in aqueous solution (Benfatto *et al.*, 1997). In addition, the XANES spectra show some dependence on the substrate, *i.e.* whereas the spectra of the 1 Eq-ML of NiO grown on both SiO_2 and Al_2O_3 are identical, within the signal-to-noise ratio, the XANES spectrum of the sample deposited on MgO exhibits both the broadening and energy shift of the main *C* structure and a subtle reduction of the intensity of the shoulder-like feature (*B*). The observed changes reveal the expected short-range order around Ni for low NiO coverages. Indeed, the main difference between the spectra obtained for the final deposition stage of NiO (bulk-like) and the early stages of deposition (nanostructures) appears at about 20 eV above the absorption edge (see Fig. 3). At these energies the XANES spectra of the 80 Eq-ML samples show a resonance-like structure (*B*) that evolves towards a shoulder-like structure in the case of the 1 Eq-ML samples. The fact that this difference is common to all of the systems, *i.e.* independent of the oxide substrate, suggests that its origin is related to the extension of the local order around the absorbing atom. In

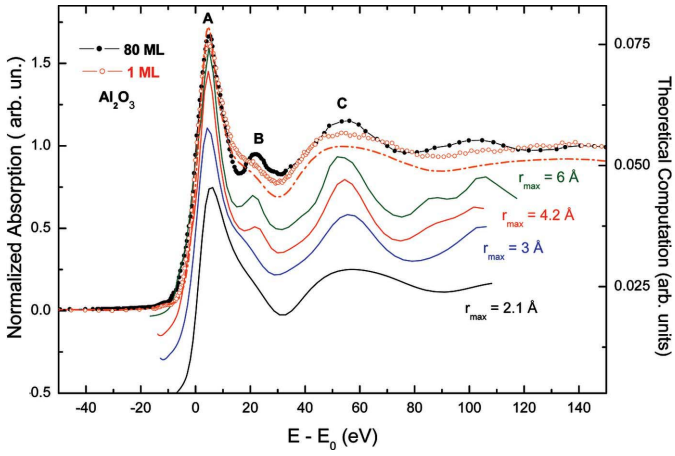

Figure 3
Comparison of the experimental Ni *K*-edge XANES spectra for 80 Eq-ML (solid dots) and 1 Eq-ML (open dots) of NiO on Al_2O_3 with the theoretical spectra calculated for NiO clusters of different size. For the sake of completeness the experimental spectrum of Ni^{2+} in aqueous solution is also shown (dot-dash line).

contrast, differences observed in the XANES spectra of the 1 Eq-ML samples suggest the influence of the substrate oxide on the conformation of the Ni—O coordination polyhedron, that can be developed through either the modification of the Ni—O interatomic distances or by the substitution of Ni by metal atoms from the substrate and the concomitant variation of the Ni—O—*M* distances. It is worth mentioning in this respect that the observed differences resemble those discussed regarding the existence of the second hydration shell in aqueous solutions of transition metals (D'Angelo *et al.*, 2006).

As commented above, the low signal-to-noise ratio of the signals prevents us from performing a detailed quantitative EXAFS analysis such as those previously reported on nanocrystalline nickel oxides (Anspoks & Kuzmin, 2011; Anspoks *et al.*, 2012). Therefore, in order to explore these possibilities we have performed different *ab initio* calculations of the Ni *K*-edge XANES spectra. In this way we have carried out several computations starting from the greatest NiO cluster (6 Å), reproducing the XANES spectrum of bulk NiO (see Fig. 1), and by decreasing progressively the coordination shells around the photoabsorbing Ni. The results of these calculations, reported in Fig. 3, clearly show how the appearance of peak *B*, as in the case of the 80 Eq-ML, is due to the presence of higher coordination shells. Indeed, it is smeared out for a cluster containing the contributions of only the first two coordination shells around Ni (*i.e.* 6 O at ∼2.07 Å and 12 Ni at 2.95 Å). These results point out that in the case of 1 Eq-ML NiO deposition the local order around Ni is limited to the first two coordination shells. The inclusion of the second coordination shell improves the agreement between the theoretical and experimental spectra of the 1 Eq-ML samples in the low-energy region, *i.e.* the intensity and shape of the shoulder-like feature *B* and the energy position of the first minimum ∼30 eV above the edge. On the contrary, the width of the *C* resonance, which is well reproduced in the case of the 80 Eq-ML samples, broadens for the 1 Eq-ML samples and this broadening is not theoretically reproduced. This failure may be an indication of the influence of the substrate either through distortions of the Ni—O first coordination shell or by the replacement of some Ni atoms in the second coordination shell by cations of the substrate.

Aiming to verify these possibilities we have performed different calculations on a NiO cluster of 19 atoms, *i.e.* including the first two coordination shells, in which the Ni atoms in the second coordination sphere are progressively substituted by the substrate metal. The results of these computations, reported in Fig. 4, support the above hypothesis. In the case that the four Ni atoms closest to the substrate are substituted by Al, the enlarged width of the *C* resonance is well accounted for by the calculation. Finally we have considered that this substitution of Ni by the substrate metal implies a distortion of the interatomic distances. Therefore we have isotropically contracted/enlarged the 19-atom NiO cluster once four Al atoms have been included in the second coordination shells substituting Ni atoms. As shown in the bottom panel of Fig. 4, the best agreement with the experimental spectra is obtained when the Ni—O—Al interatomic

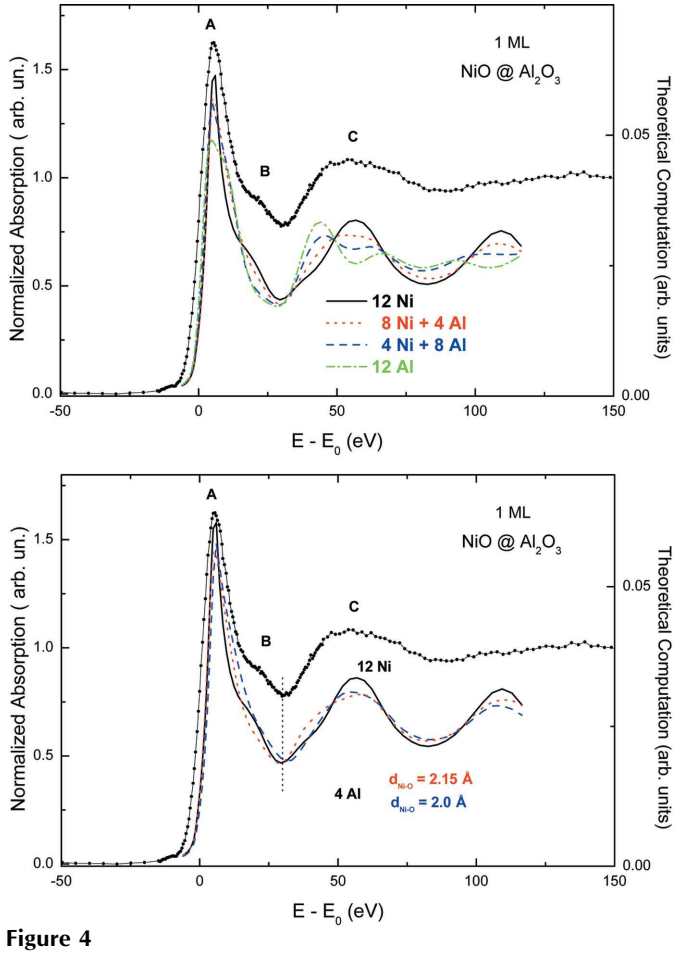

Figure 4
Top: comparison of the experimental Ni *K*-edge XANES spectrum for 1 Eq-ML (dots) of NiO on Al_2O_3 with the theoretical spectra calculated for a 19-atom cluster where Ni atoms have been substituted by Al atoms as labelled in the figure. Bottom: comparison of the experimental Ni *K*-edge XANES spectrum for 1 Eq-ML (dots) of NiO on Al_2O_3 with the theoretical spectra calculated for a 19-atom cluster with four Al atoms where the O—Al distances have been varied as labelled in the figure.

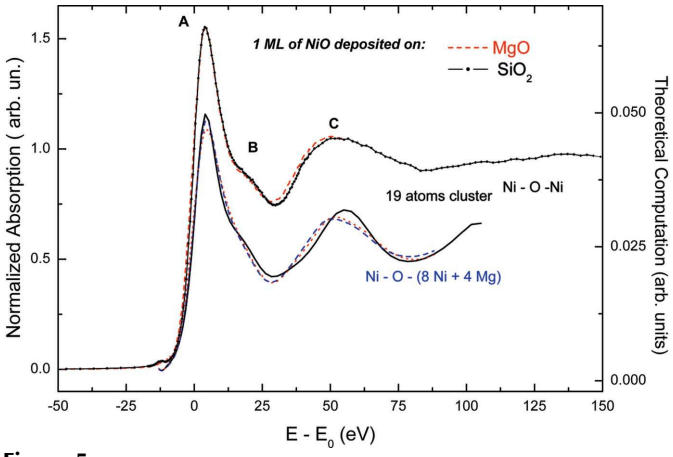

Figure 5
Comparison of the experimental Ni *K*-edge XANES spectra for 1 Eq-ML of NiO on SiO_2 and MgO and the theoretical spectra calculated for both a NiO cluster (solid line) and for a second cluster in which four Mg atoms replace Ni in the second coordination shell. In the latter case the Ni(*M*)—O interatomic distances of the first shell (dots) and both first and second shells (dashes) have been increased (see text for details).

distances enlarge with respect to the bulk Ni—O—Ni bond. The increase of the Ni—O interatomic distances implies a shift towards lower energies of the main spectral features. As shown in Fig. 2, this effect is more important for the MgO case than for both SiO_2 and Al_2O_3 substrates, in agreement with the longer Mg—O bond. Therefore we have performed similar computations of a 19-atom NiO cluster in which four Mg atoms replace Ni in the second coordination shell. The replacement of Mg by Ni atoms has been combined with an increase of the Ni—O interatomic distance up to 2.11 Å in the first shell and also by considering the increase of the Ni—Mg ones (2.98 Å). Fig. 5 reports the comparison of the theoretical spectra calculated for a NiO cluster in which four Mg atoms replace Ni in the second coordination shell and the Ni—O interatomic distances of the first shell and both first and second shells have been increased. As shown in Fig. 5, the results obtained by the simulations mimic the experimental ones. Consequently, these results are consistent with the formation of cross-linking bonds at the NiO/oxide interfaces as suggested from XPS data (Preda *et al.*, 2008).

4. Summary and conclusions

In summary, we have studied the local structure of the Ni atoms located at the interfaces formed by the deposition of NiO on selected oxides by means of the Ni XANES *K*-edge for two different coverages, *i.e.* 1 Eq-ML and 80 Eq-ML. Whereas the spectra for NiO coverages of 80 Eq-ML on all the oxide substrates are identical and agree with that of bulk NiO, the spectra corresponding to low coverages differ significantly from that of large coverages. Detailed analysis of the spectra by simulation of the Ni *K*-edge XANES spectra using multiple-scattering theory indicates that in the case of 1 Eq-ML NiO deposition the local order around Ni extends only to the first two coordination shells. In addition, these results also suggest the presence of the substrate atoms at the interface, being consistent with the formation of cross-linking bonds of the form Ni—O—*M* (*M* = Si, Al, Mg) at the interface.

This work was partially supported by the Spanish CONSOLIDER Project FUNCOAT CSD2008-00023, the ENE2010-21198-C04-04 and MAT2011-27573-C04-04 projects and by the Aragón DGA NETOSHIMA grant. We acknowledge the Spanish Ministerio de Ciencia e Innovación and CSIC for financial support and for provision of synchrotron radiation and we would like to thank the staff of SpLine at ESRF and KMC2 at BESSY II for technical support. The research leading to these results has received funding from the European Community's Seventh Framework Programme (FP7/2007-2013) under grant agreement No. 22671.

References

Ankudinov, A., Ravel, B., Rehr, J. J. & Conradson, S. D. (1998). *Phys. Rev. B*, **58**, 7565–7576.
Anspoks, A., Kalinko, A., Kalendarev, R. & Kuzmin, A. (2012). *Phys. Rev. B*, **86**, 174114.
Anspoks, A. & Kuzmin, A. (2011). *J. Non-Cryst. Solids*, **357**, 2604–2610.
Benfatto, M. & Della Longa, S. (2001). *J. Synchrotron Rad.* **8**, 1087–1094.
Benfatto, M., Solera, J. A., Chaboy, J., Proietti, M. G. & García, J. (1997). *Phys. Rev. B*, **56**, 2447–2452.
Chaboy, J. (2009). *J. Synchrotron Rad.* **16**, 533–544.
Chaboy, J. & Díaz-Moreno, S. (2011). *J. Phys. Chem. A*, **115**, 2345–2349.
Chaboy, J., Maruyama, H. & Kawamura, N. (2007*b*). *J. Phys. Condens. Matter*, **19**, 216214.
Chaboy, J., Muñoz-Páez, A., Carrera, F., Merkling, P. & Marcos, E. (2005). *Phys. Rev. B*, **71**, 134208.
Chaboy, J., Nakajima, N. & Tezuka, Y. (2007*a*). *J. Phys. Condens. Matter*, **19**, 266206.
Chaboy, J. & Quartieri, S. (1995). *Phys. Rev. B*, **52**, 6349–6357.
D'Angelo, P., Roscioni, O. M., Chillemi, G., Della Longa, S. & Benfatto, M. (2006). *J. Am. Chem. Soc.* **128**, 1853–1858.
Díaz-Moreno, S. & Chaboy, J. (2009). *J. Phys. Chem. B*, **113**, 3527–3535.
Díaz-Moreno, S., Muñoz-Páez, A. & Chaboy, J. (2000). *J. Phys. Chem. A*, **104**, 1278–1286.
Gougoussis, C., Calandra, M., Seitsonen, A., Brouder, C., Shukla, A. & Mauri, F. (2009). *Phys. Rev. B*, **79**, 045118.
Guglieri, C., Céspedes, E., Prieto, C. & Chaboy, J. (2011). *J. Phys. Condens. Matter*, **23**, 206006.
Guglieri, C. & Chaboy, J. (2010). *J. Phys. Chem. C*, **114**, 19629–19634.
Hatada, K. & Chaboy, J. (2007). *Phys. Rev. B*, **76**, 104411.
Horcas, I., Fernández, R., Gómez-Rodríguez, J. M., Colchero, J., Gómez-Herrero, J. & Baro, A. M. (2007). *Rev. Sci. Instrum.* **78**, 013705.
Joly, Y. (2001). *Phys. Rev. B*, **63**, 125120.
Krause, M. O. & Oliver, J. H. (1979). *J. Phys. Chem. Ref. Data*, **8**, 329.
Kuzmin, A., Mironova, N., Purans, J. & Rodionov, A. (1995). *J. Phys. Condens. Matter*, **7**, 9357–9368.
Kuzmin, A., Purans, J. & Rodionov, A. (1997). *J. Phys. Condens. Matter*, **9**, 6979–6993.
Meneses, C. T., Flores, W. H. & Sasaki, J. M. (2007). *Chem. Mater.* **19**, 1024–1027.
Natoli, C. R. & Benfatto, M. (1986). *J. Phys. (Paris) Colloq.* **47**, C8–11.
Preda, I., Gutiérrez, A., Abbate, M., Yubero, F., Méndez, J., Alvarez, L. & Soriano, L. (2008). *Phys. Rev. B*, **77**, 075411.

Ravel, B. & Newville, M. (2005). *J. Synchrotron Rad.* **12**, 537–541.
Sánchez-Agudo, M., Soriano, L., Quirós, C., Avila, J. & Sanz, J. M. (2001). *Surf. Sci.* **482–485**, 470–475.
Sayers, D. E. & Bunker, B. A. (1988). *X-ray Absorption: Principles, Applications, Techniques of EXAFS, SEXAFS, and XANES*, ch. 6. New York: Wiley.
Soriano, L., Fuentes, G. G., Quirós, C., Trigo, J. F., Sanz, J. M., Bressler, P. R. & González-Elipe, A. R. (2000). *Langmuir*, **16**, 7066–7069.
Soriano, L., Sánchez-Agudo, M., Mossanek, R. J. O., Abbate, M., Fuentes, G. G., Bressler, P. R., Alvarez, L., Méndez, J., Gutiérrez, A. & Sanz, J. M. (2011). *Surf. Sci.* **605**, 539–544.
Tougaard, S. (1994). *QUASES Software packages to characterize surface nano-structures by analysis of electron spectra*, http://www.QUASES.com.
Vedrinskii, R. V., Kraizman, V. L., Novakovich, A. A., Elyafi, Sh. M., Bocharov, S., Kirchner, Th. & Dräger, G. (2001). *Phys. Status Solidi B*, **226**, 203–217.